

Edge-Forming Methods for Image Zooming: Color Images

Youngjoon Cha and Seongjai Kim

Abstract

This article introduces edge-forming schemes for image zooming of color images by general magnification factors. In order to remove/reduce artifacts arising in image interpolation such as image blur and the checkerboard effect, an edge-forming method is suggested to be applied as a post-process of standard interpolation methods. The method is based on non-convex nonlinear partial differential equations. The equations are carefully discretized, incorporating numerical schemes of anisotropic diffusion, to be able to form reliable edges satisfactorily. The alternating direction implicit (ADI) method is employed for an efficient simulation of the model. It has been numerically verified that the resulting algorithm can form clear edges in 2-3 ADI iterations. Various results are given to show effectiveness and reliability of the algorithm.

Key words. Image zooming, interpolation, checkerboard effect, edge-forming.

Mathematical subject classifications. 35K55, 65M06, 65M12

I. INTRODUCTION

Image interpolation is the first of two basic resampling steps and turns a discrete image into a continuous function, which is necessary for various geometric transform of discrete images. There are two kinds of interpolation methods: linear and nonlinear ones. For linear methods, diverse interpolation kernels of finite size have been introduced, in the literature, as approximations of the *ideal* interpolation kernel (the sinc function) which is spatially unlimited; see [11], [17], [28]. Two of the simplest approximations are related to the nearest-neighbor interpolation and the bilinear interpolation. Higher-order interpolation methods involving larger number of pixel values have shown superior properties for some classes of images. However, most of the linear interpolation methods have been introduced without considering specific (local) information of edges. Thus they bring up the smoothing effect in resulting images. Furthermore, when the image is zoomed by a large factor, the zoomed image looks blocky; such a phenomenon is called the

Department of Applied Mathematics, Sejong University, 98 Kunja-Dong, Seoul, 143-747, South Korea Email: yjcha@sejong.ac.kr

Department of Mathematics, University of Kentucky, Lexington, Kentucky 40506-0027 USA Email: skim@ms.uky.edu. The work of this author is supported in part by NSF grant DMS-0312223.

checkerboard effect. Recently, some nonlinear interpolation methods have been suggested to reduce the artifacts of linear methods [3], [13], [18]. The major step in the nonlinear methods is to either fit the edges with some templates or predict edge information for the high resolution image from the low resolution one.

A color image is usually represented as a $3D$ vector such that each components represents intensity of RGB (red, green, and blue) three colors. For color image denoising, we first observe the work of Sapiro and Ringach [24] and Blomgren and Chan [1], [2]. Recently, the variational method has been generalized to non-flat features [5], [6], [16], [22], [25], [26], [27].

In this article, we are interested in the development of edge-forming methods to be applied as a post-process of standard image zooming methods for color images, with a hope of removing the checkerboard effect. As the model, we consider a system of nonlinear partial differential equations (PDEs) in the angle domain, which can be viewed as a variant of the model in Vese and Osher [29]. Then separable anisotropic numerical schemes are incorporated for the model to form reliable edges. The alternating direction implicit (ADI) method is adopted to compute the resulting algebraic system efficiently.

For a closely related method, see a total variation (TV)-based interpolation method suggested by Guichard and Malgouyres [12]. See also [19], where some linear and nonlinear interpolation methods are analyzed mathematically and experimentally, including the TV-based interpolation.

An outline of the article is as follows. In the next section, we briefly review the anisotropic edge-forming method for gray-scale images, which has been suggested by the authors [4]. Section III contains an extension of the edge-forming method for color images. For a choice of edge-forming model, we have modified the model of Vese and Osher [29], which was first introduced for p -harmonic flows and its application to denoising. The ADI method is employed, as an iterative procedure for the integration in the direction of artificial time. In Section IV, a new constraint parameter is considered in order for the new algorithm to be able to form edges for image zooming by general (non-integer) magnification factors. Section V shows numerical experiments; our new algorithm turns out to be able to form clear edges for various color images, satisfactorily in 2-3 ADI iterations. The last section concludes our development and experiments.

II. PRELIMINARIES

In this section, we briefly review an effective edge-forming technique, suggested by the authors [4], as a post-process of standard interpolation methods for gray-scale images.

A. A semi-discrete model

Let u^0 be a given image which is zoomed by one of linear interpolation methods. Then we can write

$$u^0 = u + r,$$

where u is the desired image (hopefully, having sharp and reliable edges) and r denotes the noise involved during the interpolation and resampling. Consider the semi-discrete model of the form

$$\frac{\partial u}{\partial t} + \mathcal{A}u = \beta(u^0 - u), \quad (1)$$

where β denotes a constraint parameter and $\mathcal{A} = \mathcal{A}(u)$ is a *diffusion* matrix, i.e., for $\mathcal{A} = (a_{rs})$,

$$a_{rs} \leq 0, \quad r \neq s; \quad a_{rr} = \sum_{s \neq r} |a_{rs}| > 0, \quad \forall r.$$

The diffusion must be anisotropic and carefully designed in order to preserve and construct reliable edges.

Note that the recovered image u becomes closer to u^0 as β grows. When images are to be magnified by an integer factor $k_1 \times k_2$, one can manage the interpolation algorithm such that the values at each $(k_1 \times k_2)$ -th pixel can be assigned directly from the original image without approximation. It is then desirable that we try not to alter those original values during the post-processing of edge-forming. Thus we may set β in (1) large at the pixels of original values and let $\beta = 0$ elsewhere. In this article, such β is said to be *two-valued*.

For an efficient simulation of (1), we will select \mathcal{A} separable, i.e.,

$$\mathcal{A} = \mathcal{A}_1 + \mathcal{A}_2,$$

where \mathcal{A}_1 and \mathcal{A}_2 are submatrices that represent connections of pixel values in the horizontal and vertical directions, respectively. In Section II-B, we will show an explicit construction of the diffusion matrix that shows an ability to form edges. We first consider an efficient (linearized) time-stepping procedure for (1).

Denote the timestep size by Δt . Set $t^n = n\Delta t$ and $u^n = u(\cdot, t^n)$ for $n \geq 0$. Then, the problem can be linearized by evaluating the matrix $\mathcal{A}(u)$ from the previous time level. Consider the linearized θ -method for (1) of the form:

$$\frac{u^n - u^{n-1}}{\Delta t} + (\mathcal{A}^{n-1} + \beta I) [\theta u^n + (1 - \theta)u^{n-1}] = \beta u^0, \quad 0 \leq \theta \leq 1, \quad (2)$$

where $\mathcal{A}^{n-1} = \mathcal{A}(u^{n-1})$. Note that the θ -method turns out to be the explicit, the implicit, and the Crank-Nicolson methods respectively for $\theta = 0$, $\theta = 1$, and $\theta = 1/2$. Let

$$\mathcal{B}_\ell^{n-1} = \mathcal{A}_\ell^{n-1} + \frac{1}{2}\beta I, \quad \ell = 1, 2.$$

Then, the *alternating direction implicit* (ADI) method [7], [8], [9], [10], [21] is a perturbation of (2), with a splitting error of $\mathcal{O}(\Delta t^2)$:

$$\begin{aligned} [1 + \theta \Delta t \mathcal{B}_1^{n-1}] u^* &= [1 - (1 - \theta) \Delta t \mathcal{B}_1^{n-1} - \Delta t \mathcal{B}_2^{n-1}] u^{n-1} + \Delta t \beta u^0, \\ [1 + \theta \Delta t \mathcal{B}_2^{n-1}] u^n &= u^* + \theta \Delta t \mathcal{B}_2^{n-1} u^{n-1}, \end{aligned} \quad (3)$$

where u^* is an intermediate solution. Note that when the matrices \mathcal{A}_ℓ^{n-1} are composed with a 3-point stencil, each sweep in (3) can be carried out by inverting a series of tri-diagonal matrices.

B. Edge-forming schemes

We will consider an effective edge-forming scheme for \mathcal{A}_1 for anisotropic diffusion (AD); it is straightforward to apply the same scheme for \mathcal{A}_2 .

Let \mathbf{x}_{ij} be the ij -th pixel in the image and $u_{ij} = u(\mathbf{x}_{ij})$. We construct the row of \mathcal{A}_1^{n-1} corresponding to the pixel \mathbf{x}_{ij} , $[\mathcal{A}_1^{n-1}]_{ij}$, which consists of three consecutive non-zero elements which represent the connection of u_{ij} to $u_{i-1,j}$ and $u_{i+1,j}$:

$$[\mathcal{A}_1^{n-1}]_{ij} = (-a_{ij,W}^{n-1}, a_{ij,W}^{n-1} + a_{ij,E}^{n-1}, -a_{ij,E}^{n-1}), \quad (4)$$

where

$$a_{ij,W}^{n-1} = \frac{2 d_{ij,E}^{n-1}}{d_{ij,W}^{n-1} + d_{ij,E}^{n-1}}, \quad a_{ij,E}^{n-1} = \frac{2 d_{ij,W}^{n-1}}{d_{ij,W}^{n-1} + d_{ij,E}^{n-1}}. \quad (5)$$

We wish to determine $d_{ij,E}^{n-1}$ and $d_{ij,W}^{n-1}$ in such a way that the algorithm (2) can form edges. Let

$$d_{ij,W}^{n-1} = [(\mathcal{D} u_{i-1/2,j}^{n-1})^2 + \varepsilon^2]^{q/2}, \quad d_{ij,E}^{n-1} = d_{i+1,j,W}^{n-1}, \quad q \geq 0, \quad (6)$$

where the regularization parameter $\varepsilon > 0$ has been introduced to prevent the denominator in (4) from approaching zero and $\mathcal{D} u_{i-1/2,j}^{n-1}$ is to be defined as finite difference approximations of $|\nabla u^{n-1}|$ evaluated at $\mathbf{x}_{i-1/2,j}$, the mid point of $\mathbf{x}_{i-1,j}$ and $\mathbf{x}_{i,j}$:

$$\begin{aligned} &\mathcal{D} u_{i-1/2,j}^{n-1} \\ &= \left((u_{i,j}^{n-1} - u_{i-1,j}^{n-1})^2 + \left[\frac{1}{2} \left(\frac{u_{i-1,j+1}^{n-1} + u_{i,j+1}^{n-1}}{2} - \frac{u_{i-1,j-1}^{n-1} + u_{i,j-1}^{n-1}}{2} \right) \right]^2 \right)^{1/2} \\ &= \left((u_{i,j}^{n-1} - u_{i-1,j}^{n-1})^2 + (u_{i-1,j+1}^{n-1} + u_{i,j+1}^{n-1} - u_{i-1,j-1}^{n-1} - u_{i,j-1}^{n-1})^2 / 16 \right)^{1/2}. \end{aligned} \quad (7)$$

The numerical realization of the model (1), the θ -method (2) incorporating the schemes (4)-(7), has showed an excellent performance for edge-forming for 2D images when $q \in [1.3, 1.8]$. The authors [4] analyzed stability for the θ -method as in the following two theorems.

Theorem 2.1. [4] *Suppose that the image is to be magnified by a factor of $k_1 \times k_2$, where k_1 and k_2 are positive integers. Let the θ -method (2), $0 \leq \theta \leq 1$, incorporate the edge-forming schemes (4)-(7) and satisfy the following condition*

$$4(1 - \theta)\Delta t \leq 1. \quad (8)$$

Suppose the solution of (2), u^n , have a local maximum or minimum at a point $\hat{\mathbf{x}}_{ij}$ where $\beta = 0$. Then it is constant, for all $q \geq 0$, on the block of $(k_1 \times k_2)$ pixels that contains the point $\hat{\mathbf{x}}_{ij}$.

Theorem 2.2. [4] *Let the θ -method (2), $0 \leq \theta \leq 1$, incorporate the edge-forming schemes (4)-(7) and satisfy*

$$\theta \geq \frac{1}{2}, \quad (4 + \beta)(1 - \theta)\Delta t \leq 1. \quad (9)$$

Then,

$$\max_{\beta > 0} |u_{ij}^n - u_{ij}^0| \leq \frac{4}{4 + \beta} \|u^0\|_\infty, \quad n \geq 1. \quad (10)$$

For instance, if it is desired for $|u_{ij}^n - u_{ij}^0|$ to be not larger than 1% the given image u^0 at the pixels where $\beta > 0$, one should choose $\beta \geq 396$. (For the numerical results in Section V, we set $\beta = 1000$ for the two-valued β .)

III. EDGE-FORMING METHODS FOR COLOR IMAGES

A. An interpretation for the semi-discrete model

We begin with a numerical interpretation for the semi-discrete model (1) and the edge-forming schemes (4)-(7), from which we will try to obtain motivation for an effective model for color image zooming. The schemes can be obtained from a numerical approximation of a diffusion operator of the term

$$-|\nabla u^{n-1}|_\varepsilon^q \left(\frac{u_x^n}{|\nabla u^{n-1}|_\varepsilon^q} \right)_x, \quad q \geq 0,$$

where $|\nabla u|_\varepsilon = \sqrt{u_x^2 + u_y^2 + \varepsilon^2}$. Indeed, the scheme can be obtained with the following differences:

$$\begin{aligned} \left(\frac{u_x^n}{|\nabla u^{n-1}|_\varepsilon^q} \right)_x (\mathbf{x}_{ij}) &\approx \frac{1}{d_{ij,W}^{n-1}} u_{i-1,j}^n - \left(\frac{1}{d_{ij,W}^{n-1}} + \frac{1}{d_{ij,E}^{n-1}} \right) u_{ij}^n + \frac{1}{d_{ij,E}^{n-1}} u_{i+1,j}^n, \\ |\nabla u^{n-1}|_\varepsilon^q (\mathbf{x}_{ij}) &\approx 2 \frac{d_{ij,W}^{n-1} \cdot d_{ij,E}^{n-1}}{d_{ij,W}^{n-1} + d_{ij,E}^{n-1}}. \end{aligned} \quad (11)$$

Thus, the discrete model (1) incorporating the anisotropic edge-forming schemes (4)-(7) can be viewed as a linearized spatial discretization of the following nonlinear PDE

$$\frac{\partial u}{\partial t} - |\nabla u|_\varepsilon^q \nabla \cdot \left(\frac{\nabla u}{|\nabla u|_\varepsilon^q} \right) = \beta(u^0 - u), \quad q \geq 0, \quad (12)$$

which is a variant of the denoising PDE model suggested by either Rudin *et al.* [23] (the TV model) or Marquina and Osher [20].

B. An edge-forming model for color images

For edge-forming schemes for color images, we have been motivated from the observation in Section III-A. In this subsection, we will first consider a denoising model for color images and then it will be modified and approximated to be able to form edges.

In the RGB representation, a color image is a mapping

$$I : \Omega \rightarrow \mathbb{R}_+^3 = \{(r, g, b) : r, g, b \geq 0\},$$

which can be decomposed into brightness and chromaticity:

$$\begin{aligned} \eta(\mathbf{x}) &= \|I(\mathbf{x})\|, & \text{(brightness)} \\ \mathbf{u}(\mathbf{x}) &= \frac{I(\mathbf{x})}{\|I(\mathbf{x})\|} = \frac{I(\mathbf{x})}{\eta(\mathbf{x})}, & \text{(chromaticity)} \end{aligned} \quad (13)$$

where $\|\cdot\|$ is the least-squares (L^2) norm. Thus the brightness η represents the length of the RGB color vector and the chromaticity \mathbf{u} denotes the normalized color component, which lies on the unit sphere S^2 . In [5] and [6], it has been verified that in denoising, the use of the chromaticity-brightness (CB) decomposition results in better restored images than conventional approaches such as the channel-by-channel model and the HSV system.

The brightness can be treated as the same way as for gray-scale images, applying the edge-forming model (1). On the other hand, we need to develop an appropriate mathematical model to handle the chromaticity effectively in the angle domain.

Based on the elegant mathematical work by Vese and Osher [29], Joo and Kim [14] have experimented an angle domain algorithm to denoise color images efficiently and reliably. Let $\mathbf{v} = \eta \mathbf{u} = (u, v, w)$ and

$$\varphi = \tan^{-1} \left(\frac{w}{\sqrt{u^2 + v^2}} \right), \quad \xi = \tan^{-1} \left(\frac{v}{u} \right).$$

(It should be noticed that $u, v, w \geq 0$ and therefore $0 \leq \varphi, \xi \leq \pi/2$; there is no difficulty for the issue of “ 2π -modulo”.) Associated with the minimization problem

$$\min_{\mathbf{v}} \int_{\Omega} \left| \nabla \left(\frac{\mathbf{v}}{|\mathbf{v}|} \right) \right|^p dx, \quad (14)$$

the Euler-Lagrange equations in the angle domain read [14], [29]

$$\begin{aligned} -\nabla \cdot \left(\frac{\nabla \varphi}{\mathcal{R}(\varphi, \xi)_\varepsilon^{2-p}} \right) &= \frac{\sin \varphi \cos \xi}{\mathcal{R}(\varphi, \xi)_\varepsilon^{2-p}} |\nabla \xi|^2, \\ -\nabla \cdot \left(\frac{\cos^2 \varphi \nabla \xi}{\mathcal{R}(\varphi, \xi)_\varepsilon^{2-p}} \right) &= 0, \end{aligned} \quad (15)$$

where

$$\mathcal{R}(\varphi, \xi)_\varepsilon = \sqrt{|\nabla \varphi|^2 + \cos^2 \varphi |\nabla \xi|^2 + \varepsilon^2}, \quad \varepsilon > 0.$$

Here we have introduced the regularization term $\varepsilon > 0$ to prevent the denominators in (15) from approaching zero.

To get an edge-forming model for the chromaticity components, we (a) multiply both sides of the equations in (15) by $\mathcal{R}(\varphi, \xi)_\varepsilon^{2-p}$, (b) introduce an artificial time t for the parameterization of the energy descent direction, and (c) impose an constraint term. It should be noticed [20] that the scaling will not make the stationary solution of the resulting model differ from that of (15) by a significant amount.

Then, the complete set of edge-forming model, including the equation for the brightness, can be formulated as follows: find (η, φ, ξ) by solving

$$\begin{aligned} \frac{\partial \eta}{\partial t} - |\nabla \eta|_\varepsilon^q \nabla \cdot \left(\frac{\nabla \eta}{|\nabla \eta|_\varepsilon^q} \right) &= \beta(\eta^0 - \eta), \\ \frac{\partial \varphi}{\partial t} - \mathcal{R}(\varphi, \xi)_\varepsilon^q \nabla \cdot \left(\frac{1}{\mathcal{R}(\varphi, \xi)_\varepsilon^q} \nabla \varphi \right) &= \sin \varphi \cos \xi |\nabla \xi|^2 + \beta(\varphi^0 - \varphi), \\ \frac{\partial \xi}{\partial t} - \mathcal{R}(\varphi, \xi)_\varepsilon^q \nabla \cdot \left(\frac{\cos^2 \varphi}{\mathcal{R}(\varphi, \xi)_\varepsilon^q} \nabla \xi \right) &= \beta(\xi^0 - \xi), \end{aligned} \quad (16)$$

where $q = 2 - p$, $\beta \geq 0$, and $(\eta^0, \varphi^0, \xi^0)$ denotes an initialization of (η, φ, ξ) .

C. Anisotropic edge-forming schemes for color images

For the discretization of the diffusion terms in the chromaticity equations in (16), we adopt the idea of the edge-forming schemes for gray-scale images presented in sections II-B and III-A. We first define $d_{ij,W}^{(c),n-1}$ and $d_{ij,E}^{(c),n-1}$, as the counterparts of $d_{ij,W}^{n-1}$ and $d_{ij,E}^{n-1}$ in (6):

$$\begin{aligned} d_{ij,W}^{(c),n-1} &= [(\mathcal{D}\varphi_{i-1/2,j}^{n-1})^2 + C_{ij,W}^{n-1} (\mathcal{D}\xi_{i-1/2,j}^{n-1})^2 + \varepsilon^2]^{q/2}, \\ d_{ij,E}^{(c),n-1} &= d_{i+1,j,W}^{(c),n-1}, \end{aligned} \quad (17)$$

where \mathcal{D} is defined as in (7) and

$$C_{ij,W}^{n-1} = \cos^2 \varphi_{i-1/2,j}^{n-1}, \quad C_{ij,E}^{n-1} = C_{i+1,j,W}^{n-1}.$$

Then, for the chromaticity components, the counterparts of $a_{ij,W}^{n-1}$ and $a_{ij,E}^{n-1}$ in (5) can be defined as

$$\begin{aligned} a_{ij,W}^{(\varphi),n-1} &= \frac{2 d_{ij,E}^{(c),n-1}}{d_{ij,W}^{(c),n-1} + d_{ij,E}^{(c),n-1}}, & a_{ij,E}^{(\varphi),n-1} &= \frac{2 d_{ij,W}^{(c),n-1}}{d_{ij,W}^{(c),n-1} + d_{ij,E}^{(c),n-1}}, & (\text{for } \varphi) \\ a_{ij,W}^{(\xi),n-1} &= \frac{2 C_{ij,W}^{n-1} d_{ij,E}^{(c),n-1}}{d_{ij,W}^{(c),n-1} + d_{ij,E}^{(c),n-1}}, & a_{ij,E}^{(\xi),n-1} &= \frac{2 C_{ij,E}^{n-1} d_{ij,W}^{(c),n-1}}{d_{ij,W}^{(c),n-1} + d_{ij,E}^{(c),n-1}}. & (\text{for } \xi) \end{aligned} \quad (18)$$

The above and (5) complete the construction of $[\mathcal{A}_1^{(\phi),n-1}]_{ij}$ as in (4), where ϕ denotes η , φ , or ξ . One can construct $[\mathcal{A}_2^{(\phi),n-1}]_{ij}$ similarly.

Thus, for each component, one can compute the solution in the new level, ϕ^n , by employing the ADI (3) as follows:

$$\begin{aligned} [1 + \theta \Delta t \mathcal{B}_1^{(\phi),n-1}] \phi^* &= [1 - (1 - \theta) \Delta t \mathcal{B}_1^{(\phi),n-1} - \Delta t \mathcal{B}_2^{(\phi),n-1}] \phi^{n-1} \\ &\quad + \Delta t (Q^{(\phi),n-1} + \beta \phi^0), \\ [1 + \theta \Delta t \mathcal{B}_2^{(\phi),n-1}] \phi^n &= \phi^* + \theta \Delta t \mathcal{B}_2^{(\phi),n-1} \phi^{n-1}, \end{aligned} \quad (19)$$

where $\mathcal{B}_\ell^{(\phi),n-1} = \mathcal{A}_\ell^{(\phi),n-1} + \beta/2$, $\ell = 1, 2$, and

$$Q^{(\eta),n-1} = Q^{(\xi),n-1} = 0, \quad Q^{(\varphi),n-1} = \sin \varphi^{n-1} \cos \xi^{n-1} |\nabla_h \xi^{n-1}|^2.$$

Here ∇_h denotes a finite difference approximation of ∇ . (In this article, we adopt the second-order central scheme for it.) We will call (19) the θ -ADI.

Remark. When the image is magnified by a large factor, e.g., 8×8 , one may try to enlarge the image by three recursive applications of 2×2 magnification and edge-forming rather than once 8×8 magnification followed by edge-forming. For the interpolation alone, a recursive application introduces no observable improvement/difference from the image of one-time application, for most cases. On the other hand, the edge-forming algorithm turns out to be able to develop reliable edges in 2-3 θ -ADI iterations for image zooming by magnification factors of 2-3, while it requires a relatively larger number of iterations for image zooming by factors ≥ 4 . Thus, one can speed up the simulation by a recursive application of smaller factors, because the earlier recursions are applied to smaller images and therefore much more efficient in computation. It also has been verified for recursive applications of edge-forming to improve the quality of resulting images; see [4].

IV. A NEW CHOICE OF β

When the image is magnified by a factor of $k_1 \times k_2$, where k_1 and k_2 are positive integers, one can manage the interpolation algorithm such that the values at each $(k_1 \times k_2)$ -th pixel can

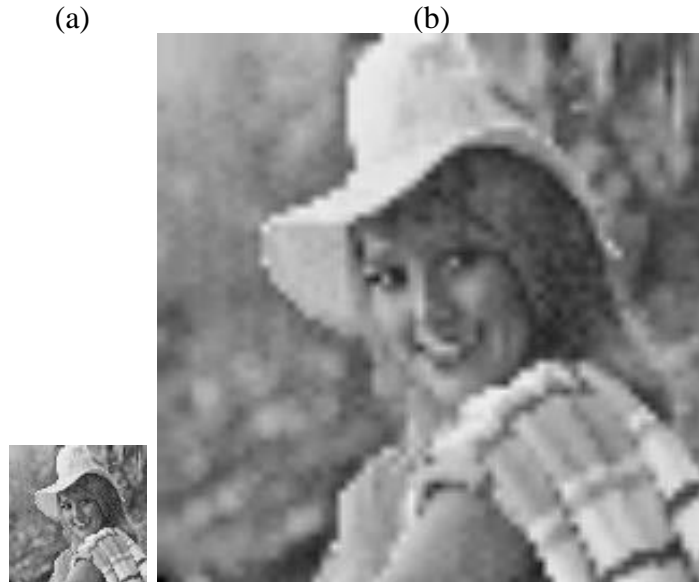


Fig. 1. Gray-scale Lenna images: (a) the original image in 64×64 pixels and (b) the magnified image by the bilinear interpolation by a factor of 4×4 .

be assigned directly from the original image without approximation. Then, we must set β in (1) large at the pixels of original values not to alter them; see Theorem 2.2. At other pixels, one may set β small or simply zero, which allows the values alter easily. However, such a strategy might not be applicable for image zooming by general (non-integer) factors, because it is rare for the values in the original image to be directly assigned to the zoomed image without approximation. In this section, we will introduce an effective strategy to overcome the difficulty.

We begin with an observation on the checkerboard effect. For simplicity, consider a gray-scale image which is magnified by the *bilinear* interpolation by an integer factor, as in Figure 1. The checkerboard effect appeared in the interpolated image, Figure 1(b), is originated from the image blocks on each of which the image is bilinear. Consider the quantity $|\Delta \phi^0|$, where Δ denotes the Laplacian and ϕ^0 is the interpolated image. Then, it is not difficult to verify that for each image blocks, the quantity must be zero at interior pixels and its local maximum appears at one of the four corner points. The more dramatic changes the image has, the larger the Laplacian is at the corners (and the sides) of the image blocks.

The above observation has motivated an effective strategy for the choice of β , given as follows:

$$\beta^{(\phi)} = \alpha |\Delta \phi^0|^\delta, \quad (20)$$

where α and δ are positive parameters to be determined and ϕ is η , φ , or ξ . The parameter α is introduced for a global scaling of β , while δ must put an emphasis of β on the corner pixels

when $\delta > 1$. Unfortunately, we do not know of any rigorous analysis for the choice of α and δ . Here is a guideline for their choices from various numerical experiments: set $\delta = 3 \sim 5$ and choose α such that the maximum of β is about 1000. (For the numerical results presented in Section V, we set $\delta = 4$ and select the scaling factor α such that $\max_{ij} \beta_{ij} = 1000$ for each of the three color components.)

Note that the strategy in (20) does not require information on the pixels whether the image values are original or not; it works along with information integrated from the image Laplacian only. With the strategy, every bilinear image block is a candidate for modification to form reliable edges, based on the minimization principle in (14). Thus there is no guarantee to set β sufficiently large to tightly keep the original image values during the edge-forming. However, since β is relatively large at pixels where the image content varies rapidly, and since the edge-forming schemes in §III-C can form reliable edges *fast*, the strategy is applicable for various situations, in particular, for image zooming by general (non-integer) magnification factors. In this article, we call the parameter β in (20) the *image-Laplacian constraint* (ILC) parameter.

When the image is magnified by a *bicubic* interpolation, the Laplacian now may not be zero at the interior pixels of image blocks. Thus one may consider the quantity $|(\partial_x^4 + \partial_y^4) \phi^0|$ for the place of $|\Delta \phi^0|$, which guarantees β to become zero at the interior pixels of image blocks. However, the Laplacian is still a favorable choice for β ; it has been experimentally verified that the ILC parameter is better than the one from the fourth-order differential operator for most real images we have tested.

V. NUMERICAL EXPERIMENTS

This section presents numerical experiments carried out with the θ -ADI (19), the edge-forming schemes discussed in Section III-C, and the parameter choice in Section IV. We select $q = 1.7$ in (17) and $\Delta t = 1.78$ and $\theta = 0.5$ for the θ -ADI. See [15] for the choice of Δt .

In Figure 2, we test performances of the new edge-forming algorithm performing for a synthetic color image. Figure 2(a) is the original image containing 60×60 pixels and it is magnified by 8×8 by a bicubic interpolation as in Figure 2(b). Figure 2(c) and Figure 2(d) depict enlarged images obtained by three recursive applications of the 2×2 bicubic interpolation and edge-forming with the two-valued β and the ILC parameter in (20), respectively. For each recursion, three θ -ADI iterations are applied. As one can see from the figure, the cubic interpolation has revealed a severe checkerboard effect and the edge-forming algorithm can form reliable edges in just three θ -ADI iterations, with the ILC parameter performing better than the

TABLE I
A PSNR ANALYSIS.

Image Zooming		Figure 6(a)	Figure 6(b)	Figure 6(c)
Cubic	2×2	28.4	26.7	32.8
	4×4	24.6	22.9	26.2
Cubic+AD	2×2	30.5	27.7	32.9
	4×4	26.4	23.8	26.4

two-valued β .

In Figure 3, we continue investigating the performance of the edge-forming algorithm for a real image, Plum, in 85×85 pixels. We have carried out the same experiment as in Figure 2, except setting the magnification factor 4×4 . Consequently, two recursive applications of 2×2 magnification are applied for image zooming and edge-forming. For real images, we have reached at the same conclusion for the performance of the edge-forming algorithm as in Figure 2. It is efficient and its results are reliable; the ILC parameter in (20) performs satisfactorily and better than the two-valued parameter.

For numerical results in the remainder of the section, we utilize the ILC (20) for the constraint parameter.

In Figure 4, we present an example for the performance of the anisotropic edge-forming algorithm for general magnification factors. The original Lenna Face is in 100×100 pixels and it is magnified by $\sqrt{14} \times \sqrt{14}$ by the bicubic interpolation as depicted in Figure 4(b). (The enlarged image is in 374×374 pixels.) The interpolated image is utilized to get an edge-formed image, Figure 4(c). As one can see from the figure, the edge-forming algorithm has eliminated the checkerboard effect in the interpolated image and formed reliable edges. For this example, each of pixel values in Figures 4(b) and 4(c) is approximated; none of them are directly assigned from the original image.

Figure 5 contains images of Cat Face. The original image is in 60×65 pixels and it is magnified by $2\pi \times 2\pi$, by the bicubic interpolation, Figure 5(b), and by two recursive applications ($\pi \times \pi$ followed by 2×2) of zooming and edge-forming, Figure 5(c). As expected, the edge-formed image shows clear and reliable edges, although some texture information for hair has been missed during the anisotropic diffusion of edge-forming.

For a more systematic analysis for the edge-forming algorithm, we shrink a selected set of images (see Figure 6) by 2×2 or 4×4 , magnify by the same factors, and then measure the

peak signal-to-noise ratio (PSNR) defined as

$$\text{PSNR} \equiv 10 \log_{10} \left(\frac{\sum_{ij} 255^2}{\sum_{ij} (I_{ij}^0 - I_{ij})^2} \right) \text{ dB},$$

where I^0 is the original image and I denotes the recovered image. As shown in Table V, the edge-forming algorithm improves the PSNR for all cases. The improvement is greatest for the gray-scale synthetic image in Figure 6(a), while the improvement for the real image in Figure 6(c) is negligible. We believe that it is due to a denoising feature of the algorithm. The image is denoised during the edge-forming operations. However, the edge-formed images have shown clear edges as in previous examples; the anisotropic edge-forming algorithm improves the image quality significantly, in practice.

VI. CONCLUSIONS

In image zooming, the image is first interpolated and then resampled for higher-resolution images. This article has introduced an new edge-forming algorithm to remover/reduce artifacts (such as image blur and the checkerboard effect) arising in image interpolation for color images. The method is based on nonlinear PDEs which are resulted from the minimization of a non-convex functional of the image gradient. Anisotropic diffusion has been incorporated through the numerical discretization of the model. For an efficient simulation of the model, we have employed the alternating direction implicit (ADI) method which is known to be very efficient in solving diffusion equations defined on rectangular domains. A new choice has been considered for the constraint parameter to be able to form edges for image zooming by general (possibly, non-integer) magnification factors. The resulting algorithm has been tested for various synthetic and real images; it can form reliable edges satisfactorily in 2-3 ADI iterations for image zooming by integer and non-integer factors, for both gray-scale and color images.

REFERENCES

- [1] P. V. Blomgren, "Total Variation Methods for Restoration of Vector Valued Images, (Ph.D. thesis)," *UCLA Dept. of Math. CAM 98-30*, 1998.
- [2] P. V. Blomgren and T. F. Chan, "Color TV: Total Variation Methods for Restoration of Vector Valued Images," *IEEE Trans. Image Processing*, vol. 7, no. 3, pp. 304–309, 1998.
- [3] W. Carey, D. Chuang, and S. Hemami, "Regularity-preserving image interpolation," *IEEE Trans. Image Process.*, vol. 8, no. 9, pp. 1293–1297, 1999.
- [4] Y. Cha and S. Kim, "Edge-forming methods for image zooming," (submitted to *J. Mathematical Imaging and Vision*).
- [5] T. F. Chan, S. H. Kang, and J. Shen, "Total Variation Denoising and Enhancement of Color Images Based on the CB and HSV Color Models," *Journal of Visual Communication and Image Representation*, vol. 12, pp. 422–435, 2001.
- [6] T. F. Chan and J. Shen, "Variational restoration of non-flat image features: Models and algorithms," *SIAM Journal of Applied Mathematics*, vol. 61, no. 4, pp. 1338–1361, 2000.
- [7] J. Douglas, Jr., "On the numerical integration of $\frac{\partial^2 u}{\partial x^2} + \frac{\partial^2 u}{\partial y^2} = \frac{\partial u}{\partial t}$ by implicit methods," *J. Soc. Indust. Appl. Math.*, vol. 3, pp. 42–65, 1955.

- [8] J. Douglas, Jr. and J. Gunn, "A general formulation of alternating direction methods Part I. Parabolic and hyperbolic problems," *Numer. Math.*, vol. 6, pp. 428–453, 1964.
- [9] J. Douglas, Jr. and S. Kim, "Improved accuracy for locally one-dimensional methods for parabolic equations," *Mathematical Models and Methods in Applied Sciences*, vol. 11, pp. 1563–1579, 2001.
- [10] J. Douglas, Jr. and D. Peaceman, "Numerical solution of two-dimensional heat flow problems," *American Institute of Chemical Engineering Journal*, vol. 1, pp. 505–512, 1955.
- [11] R. Gonzalez and R. Woods, *Digital Image Processing, 2nd Ed.* Upper Saddle River, New Jersey: Prentice-Hall, Inc., 2002.
- [12] F. Guichard and F. Malgouyres, "Total variation based interpolation," in *Proceedings of the Ninth European Signal Processing Conference*, Patran, Greece, 1998, pp. 1741–1744.
- [13] K. Jensen and D. Anastassiou, "Subpixel edge localization and the interpolation of still images," *IEEE Trans. Image Process.*, vol. 4, no. 4, pp. 285–295, 1995.
- [14] K. Joo and S. Kim, "PDE-based image restoration: A hybrid model and color image denoising," (to appear in *IEEE Trans. Image Processing*).
- [15] S. Kim, "Numerical modeling for the recovery of fine structures in PDE-based image denoising," (submitted to *Image and Vision Computing*).
- [16] R. Kimmel and N. Sochen, "Orientation Diffusion or How to Comb a Porcupine ?" *Special issue on PDEs in Image Processing, Computer Vision, and Computer Graphics, J. Visual Comm. Image Representation*, vol. 13, pp. 238–248, 2002.
- [17] T. Lehmann, C. Gönner, and K. Spitzer, "Survey: Interpolation methods in medical image processing," *IEEE Trans. Medical Imaging*, vol. 18, no. 11, pp. 1049–1075, 1999.
- [18] X. Li and M. Orchard, "New edge-directed interpolation," *IEEE Trans. Image Process.*, vol. 10, no. 10, pp. 1521–1527, 2001.
- [19] F. Malgouyres and F. Guichard, "Edge direction preserving image zooming: A mathematical and numerical analysis," *SIAM J. Numer. Anal.*, vol. 39, pp. 1–37, 2001.
- [20] A. Marquina and S. Osher, "Explicit algorithms for a new time dependent model based on level set motion for nonlinear deblurring and noise removal," *SIAM J. Sci. Comput.*, vol. 22, pp. 387–405, 2000.
- [21] D. Peaceman and H. Rachford, "The numerical solution of parabolic and elliptic differential equations," *J. Soc. Indust. Appl. Math.*, vol. 3, pp. 28–41, 1955.
- [22] P. Perona, "Orientation diffusion," *IEEE Trans. Image Processing*, vol. 7, no. 3, pp. 457–467, 1998.
- [23] L. Rudin, S. Osher, and E. Fatemi, "Nonlinear total variation based noise removal algorithms," *Physica D*, vol. 60, pp. 259–268, 1992.
- [24] G. Sapiro and D. Ringach, "Anisotropic diffusion of multivalued images with applications to color filtering," *IEEE Trans. Image Processing*, vol. 5, pp. 1582–1586, 1996.
- [25] N. Sochen, R. Kimmel, and R. Malladi, "A general framework for low level vision," *IEEE Trans. Image Processing*, vol. 7, no. 3, pp. 310–318, 1998.
- [26] B. Tang, G. Sapiro, and V. Caselles, "Color image enhancement via Chromaticity Diffusion," Technical report, ECE University of Minnesota, 1999.
- [27] —, "Diffusion of general data on non-flat manifolds via Harmonic maps theory: The direction diffusion case," *Int. J. of Computer Vision*, vol. 36, no. 2, pp. 149–161, 2000.
- [28] M. Unser, A. Aldroubi, and M. Eden, "Enlargement and reduction of digital images with minimum loss of information," *IEEE Trans. Image Process.*, vol. 4, pp. 247–257, 1995.
- [29] L. A. Vese and S. J. Osher, "Numerical methods for p -harmonic flows and applications to image processing," Department of Mathematics, University of California, Los Angeles, CA 90095, USA, Technical Report #01-22, August 2001, (To appear in *SIAM Numer. Anal.*).

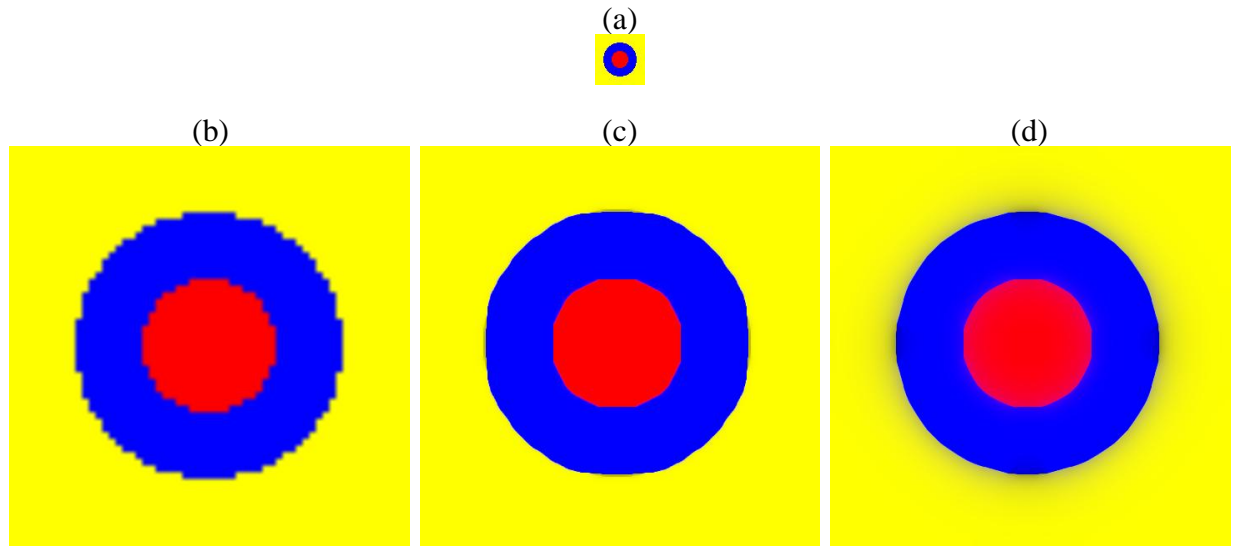


Fig. 2. Synthetic Color Disk: (a) the original image in 60×60 pixels, (b) a bicubicly interpolated image by a factor of 8×8 , (c) the edge-formed image with the two-valued β , and (d) the edge-formed image with the ILC parameter.

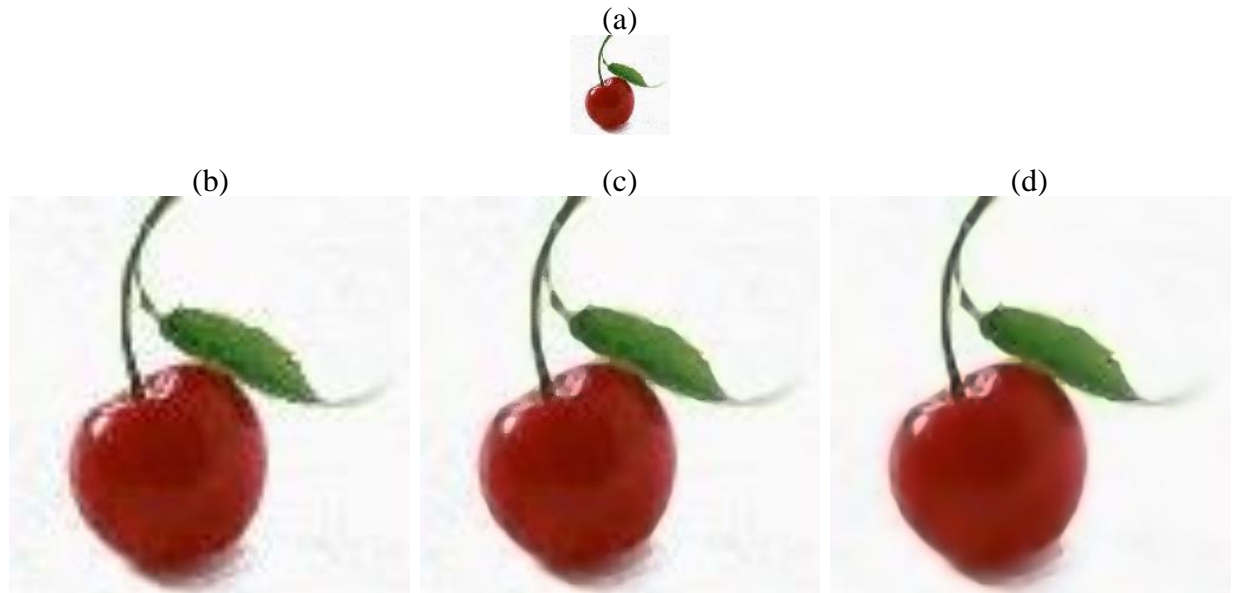


Fig. 3. A Plum: (a) the original image in 85×85 pixels, (b) a bicubicly interpolated image by a factor of 4×4 , (c) the edge-formed image with the two-valued β , and (d) the edge-formed image with the ILC parameter.



Fig. 4. Lenna: (a) the original image in 100×100 pixels, (b) a bicubically interpolated image by a factor of $\sqrt{14} \times \sqrt{14}$, and (c) the edge-formed image.

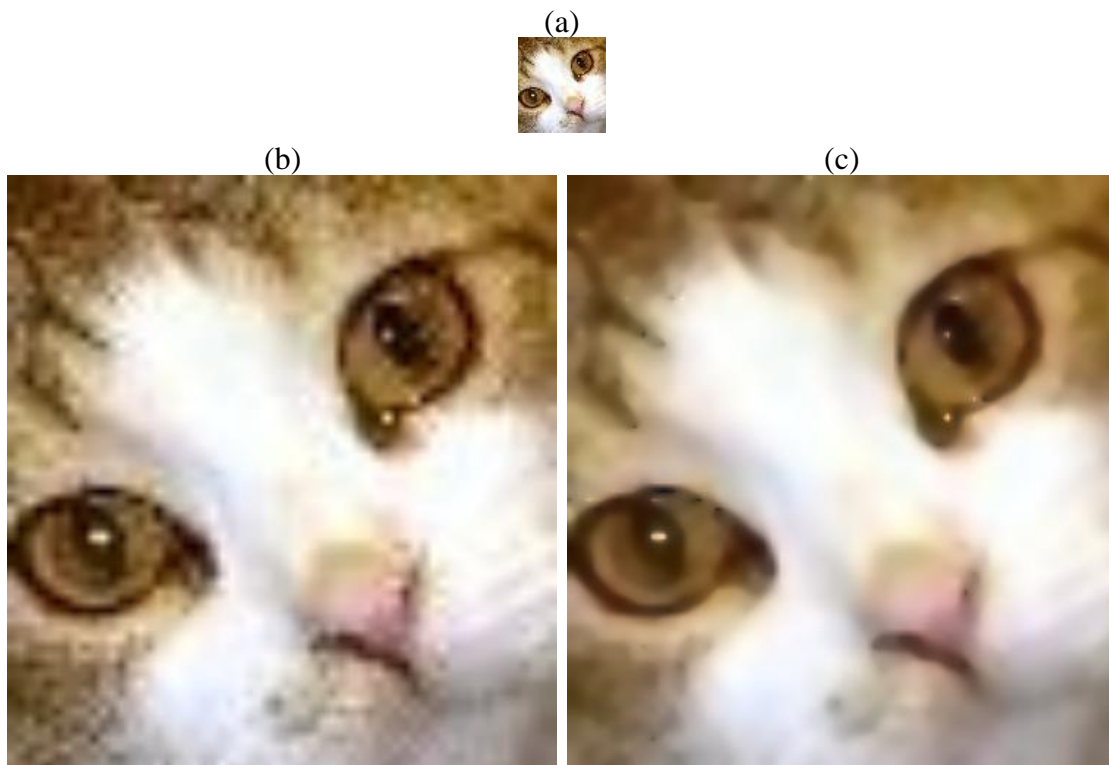


Fig. 5. Cat Face: (a) the original image in 60×65 pixels, (b) a bicubically interpolated image by a factor of $2\pi \times 2\pi$, and (c) the edge-formed image.

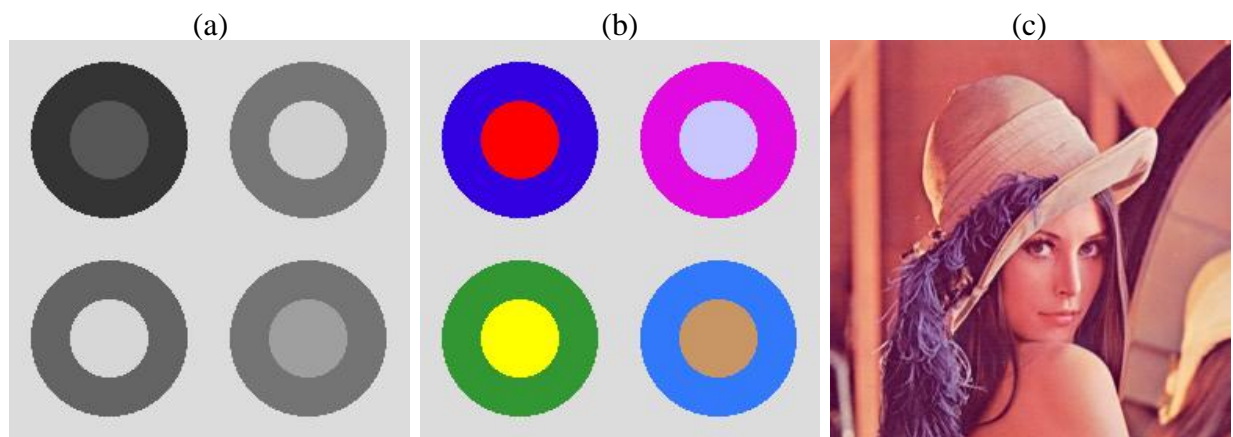


Fig. 6. Images utilized for the PSNR analysis, each in 256×256 pixels. The image in (a) is the gray-scale version of (b).